Using Machine Learning to Infer Material Properties of Debris Fragments from x-ray Images in the DebriSat Project

Saik Anam Siam[(1)], Benton R. Greene[(2)], Jonathan Sieber[(3)], Norman Fitz-Coy[(3)], and Heather M. Cowardin[(4)]

[(1)] Georgia Institute of Technology, 351 Ferst Dr. NW, Atlanta, GA 30332, USA; siam@gatech.edu
[(2)] Jacobs, NASA Orbital Debris Program Office, NASA Johnson Space Center, Mail Code XI5-9E, 2101 NASA Parkway, Houston, TX 77058, USA; benton.r.greene@nasa.gov
[(3)] University of Florida, Gainesville, FL, 32611, USA; jsieber@ufl.edu, nfc@ufl.edu
[(4)] NASA Orbital Debris Program Office, NASA Johnson Space Center, Mail Code XI5-9E, 2101 NASA Parkway, Houston, TX 77058, USA; heather.m.cowardin@nasa.gov

Abstract

The DebriSat project is a collaboration effort with the NASA Orbital Debris Program Office, the U.S. Space Force Space Systems Command Center, The Aerospace Corporation, and the University of Florida. To date, over 200,000 fragments from this ground-based, hypervelocity impact experiment have been collected, and processing is underway to determine their physical characteristics, such as material, shape, color, characteristic length, and average cross-sectional area. The x-ray process is primarily used to identify the location of the fragments and estimated size for extraction, so that these physical characteristics can be assessed. This paper proposes a machine learning-based approach to characterize materials from x-ray images of debris fragments embedded in soft-catch foam used in the DebriSat project. The novel methodology discussed in this paper will highlight the use of x-ray imagery data to characterize these fragments without extraction or a human-in-the-loop.

Both supervised and unsupervised machine learning techniques are utilized with this approach to infer the physical parameters of the fragments embedded in the soft-catch foam panels used in the impact experiment based on X-ray images of the foam panels. Additionally, 3D reconstructions of the extracted fragments are created with images taken from two different angles using the structure from motion (SfM) method. The characteristic lengths and shape from the 3D reconstruction, alongside the physical characteristics of the debris, are used in the inference of the material type.

To develop and test the approach, a dataset of x-ray images of debris fragments of varying sizes and materials is collected. Supervised learning methods such as convolutional neural networks (CNNs), support vector machines (SVM), decision trees, and random forest classifiers are used due to the high-dimensional feature spaces of the debris and nonlinear decision boundaries for material categorization. Given the limited pre-labeled data of embedded debris materials smaller than 10 mm, unsupervised machine learning techniques such as clustering algorithms and autoencoders are used, in addition to supervised learning methods. The clustering algorithms group similar fragments together based on their physical properties, and autoencoders reduce the dimensionality of the X-ray images and extract relevant features.

The performance of the proposed approach's is analyzed using a range of statistical methods, including confusion matrices, receiver operating characteristic curves, and precision-recall curves. The results are compared with those obtained using a baseline approach that relies on manual identification and classification of debris fragments. To evaluate the effectiveness of different machine learning methods, statistical tests such as t-tests, ANOVA, and cross-validation are performed, comparing the performance of CNNs, SVMs, clustering algorithms, and autoencoders. Additional analysis needs to be conducted to

identify any sources of bias or variability that may affect the results, such as variations in imaging conditions or fragmentation patterns. Other topics explored are limitations, refinements, and the potential use of semi-supervised learning techniques, such as self-training to label unlabeled datasets and co-training using X-ray images taken from two different angles as two different models.

1 Introduction

1.1 DebriSat Project

Orbital debris in the millimeter-sized range cannot be tracked, yet it is a key source of risk for missions in low Earth orbit. The NASA Orbital Debris Program Office (ODPO) uses measurements from radar, optical, and *in-situ* to develop models of the debris environment. These data are incorporated with modeling of spacecraft breakup events, along with ground-test impact experiments, to model the orbital debris environment.

DebriSat is a ground-test impact experiment performed in partnership between ODPO and the U.S. Space Force Space Systems Command, The Aerospace Corporation, and the University of Florida. This experiment has four goals: design and fabricate a 56-kg class spacecraft with modern materials representative of low Earth orbit (LEO) spacecraft, conduct a hypervelocity impact test to simulate a fragmentation event, collect and characterize fragments 2 mm and larger and use the data to improve orbital debris predictive models.

1.2 Fragment Collection and Categorization

All fragments produced from this 2014 experiment were sent to the University of Florida for characterization [1]. The NASA Standard Satellite Breakup Model (SSDM) predicted that 85,000 fragments 2 mm and larger would be produced [2]. As of September 2023, over 207,000 fragments have been recorded. Characterization of fragment parameters require precision in both analytical assessments and computed measurements. The scale of this dataset, along with parameter requirements, has led to a need to minimize human-in-the-loop assessments.

The characterization process initially uses an x-ray imager to scan the foam panels in the impact chamber, to detect and count the number of embedded fragments, and to determine size and position. Fragments ≥ 2 mm can be utilized for human-in-the-loop extraction. Post-extraction each fragment undergoes an analytical assessment to determine material type, shape, color, and whether it should be measured by a 2D or 3D imagers.

Direct mass and size [3] are measured and then used to compute volume, average cross-sectional area [4], and area-to-mass parameters. Each fragment is imaged in either the 2D or 3D Imager, based on the size of the fragment where larger fragments are imaged in 3D. The 3D imager uses photographs taken from multiple angles to reconstruct a 3D digital representation of the fragment as a triangular mesh [5]. The fragment information and measurements are then entered into the fragment database [6, 7].

Manual analysis of each debris fragment is time-intensive, so limiting manual extraction of fragments to those above a certain size threshold is necessary. An automated estimation process is needed to fill in the information gap below this size threshold. The following will highlight improvements in processing x-ray images of the foam panels using machine learning to minimize the extraction of individual fragments and provide preliminary data on all embedded fragments.

1.3 Use of X-ray Imaging in Debris Analysis

X-ray imaging enables accurate mapping of debris fragment locations within the foam panels prior to extraction. Early in the project, detection and identification of candidate fragments for extraction were performed using a medical x-ray machine at a single x-ray energy. In 2019, the machine failed, and a replacement part could not be obtained. A Transportation Security Administration Smiths Detection luggage scanner was obtained from federal government surplus, and a procedure was developed to accurately scan using the new machine [8].

Each panel is placed in a holder that keeps the panel at a known orientation within the scanner tunnel and ensures a repeatable image. Four scans of each panel are obtained at each of two panel orientations, labeled A and B. In the A view, the panel is oriented perpendicular to the direction of the x-ray beam. In the B view, the panel is rotated by 55 degrees around the long axis. Image-stacking the repeated scans and spline-fitting across pixels enables sub-millimeter detection of individual fragments within the foam. Cross-correlating detected fragments between the two views helps to reject spurious detections and improves the accuracy of size estimations for purposes of extraction prioritization. The luggage scanner also has an advantage over the previous x-ray device as it utilizes two different x-ray beams of different energies to create false color images that can be used to determine the material composition of individual fragments.

The current x-ray image processing code can perform rudimentary size and material determination sufficient to locate and extract fragments from the foam for more accurate measurement. Manually extracting each detected fragment is infeasible, thus the project prioritizes the extraction of fragments larger than 10 mm. To accurately characterize smaller fragments an improved process is needed that can accurately estimate the size and material composition of fragments using only x-ray images.

1.4 Proposed Approach

This paper proposes applying machine learning techniques to the x-ray image processing for efficient and accurate characterization of sub-10 mm debris fragments. Machine learning models could be developed to better predict material type for fragments too small to extract based on features extracted from the available multi-view x-ray images and existing size and shape data. This could enable targeted extraction of a representative sample of tiny fragments. Attempts can also be made at creating a 3D representation from the two x-ray views of each panel.

2 Fragment Analysis Methodology

In machine learning endeavors data processing is often time-consuming. This section explores the correlations inherent in the standard debris database for fragments both below and above 10 mm. It also delves into the procedures and challenges associated with accurately identifying the primary material of fragments smaller than 10 mm. Also discussed is the process of constructing a 3D representation of the debris, using information from two distinct x-ray views.

2.1 Standard Debris Database Insights

The DebriSat Debris Categorization System is a database maintained by the University of Florida to carefully catalog all DebriSat fragments and the associated data [9]. It contains the latest cumulative data of all the debris extractions for each unique fragment with a corresponding identification number.

Figure 1 shows a distribution of count and mass for each material category in the most recent DebriSat database. As depicted in the distribution, carbon fiber reinforced polymers (CFRP) represent the

majority of the fragments by raw count but a small fraction of the total mass. CFRP tends to shatter into smaller, more needle-like fragments than other materials, presenting on average a smaller depth profile to the x-ray. Epoxy resin is close in density and molecular weight to the foam than most of the other materials [10], making it difficult to detect in the x-ray images, which likely is a bias in the automated data collection that must be addressed.

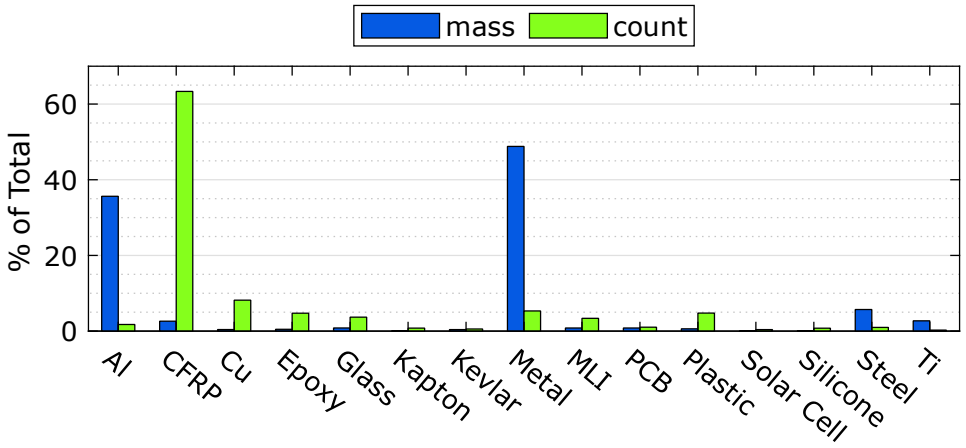

Fig 1. Distribution of material types in fragment database.

2.2 Correlations between Debris Characteristics

Categorizing based on material type, a pair-plot was created to look at what variables are highly correlated in each material category (Fig. 2). This is used to determine which variables are most predictive of material category and which only provide redundant information or are not useful.

Within the same material categories (denoted by same color), there is a high correlation between mass (m (g)) and dimension (x(mm), y(mm), and z(mm)). Since mass is a direct byproduct of material density (ρ (g/mm^3)), this high correlation is caused by material density being different in each material class. Therefore, dimensions can be used as a predictor for material. There is also a high correlation between volume (V (mm^3)) and dimensions, confirming that volume as a parameter does not add for material classification.

Figure 2 also shows that the z-dimension is heavily correlated with the x and y dimensions, demonstrating there are more debris fragments of uniform shape; therefore, similar information can be conveyed using the x and y dimensions alone. This may be useful later in choosing the appropriate characteristics of the data for training the machine learning model.

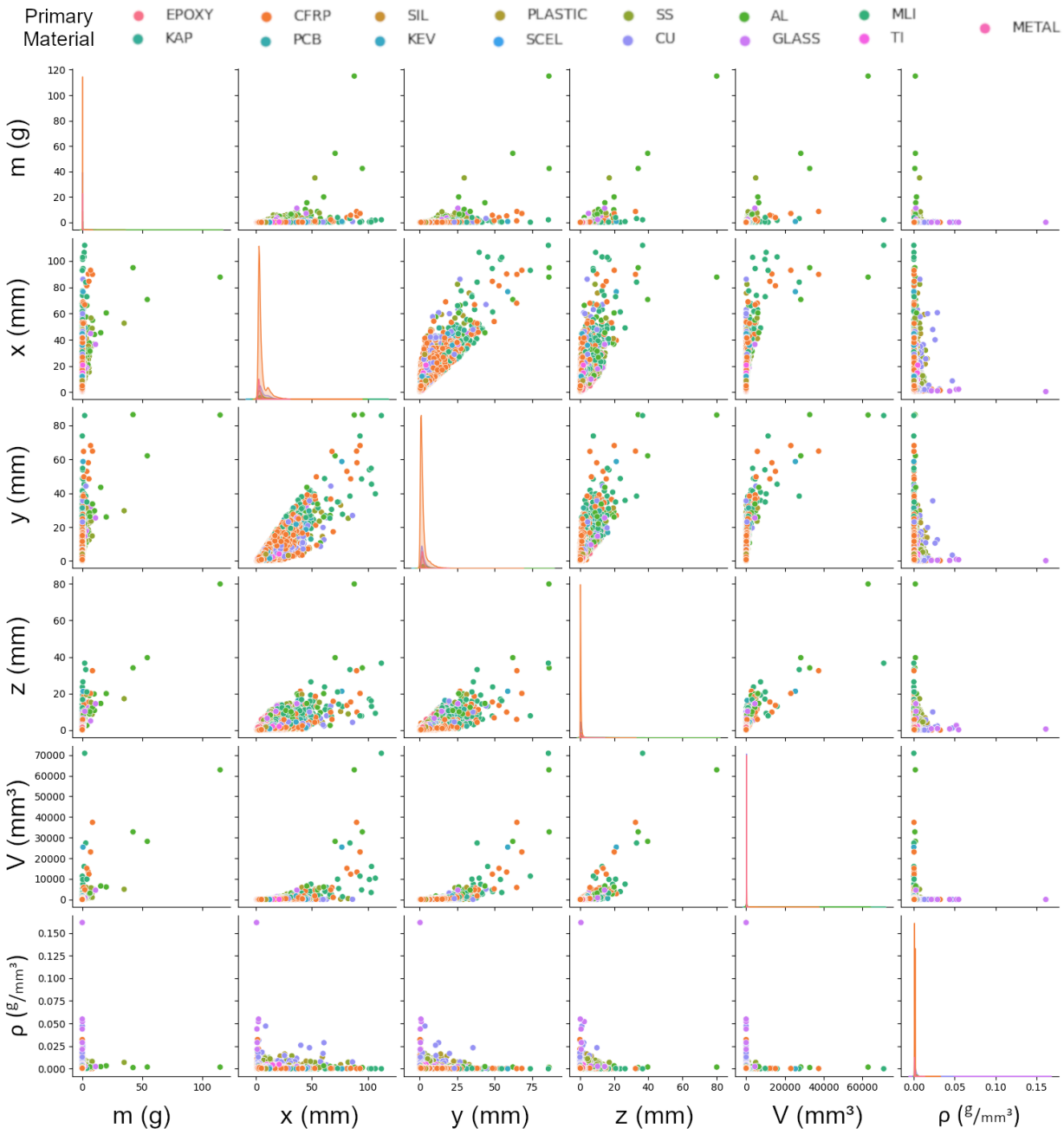

Fig 2. Pair-plot showing correlation between all the variables per material category.

2.3 X-ray Processing

The x-ray processing code is used to extract location and relevant shape descriptions of the debris from the panel x-ray images. Currently only used to determine which detected fragments are large enough for manual extraction, this new processing generates for each fragment 3D location in the foam panel, approximate length, width, and thickness, and cropped and masked x-ray images of the fragment from both the A and B views of the panel. These views are distinct x-ray images taken at two orientations 55 degrees apart and include both spatial coordinates and the false color representation of the multi-beam x-ray scan (r, g, b). As shown in Table 1, the Smiths Detection user guide provides an approximate

correlation between the false color image and the molecular weight of detected materials. The false color information in x-ray images provides insights into the material composition, while the dual-view setup aids in capturing the three-dimensional nature of the debris.

Table 1. Color Gradient on X-ray Image Depending on Atomic Number [10]

Colour gradient	eff. atomic number	pure materials and compounds
	below 10	lighter elements: hydrogen, carbon, nitrogen, oxygen and the molecular compounds of the latter, the **organic materials**: many explosives (e.g. C3H5(NO3)3 nitroglycerine), plastics such as acrylic material, paper, textiles, food, wood, water
	between 10 and 15	medium heavy elements: pure aluminum, sodium, chlorine, cooking salt
	between 15 and 56	heavier elements: the **metals** titanium, chromium, iron, nickel, copper, zinc, tin, silver etc.

Figure 3 depicts a fragment scan in both the A and B view, where the color gradient of the image is detailed by Table 1. The results of this scan suggest that the debris likely consists of a dense material with a high effective atomic number, typical of heavy materials.

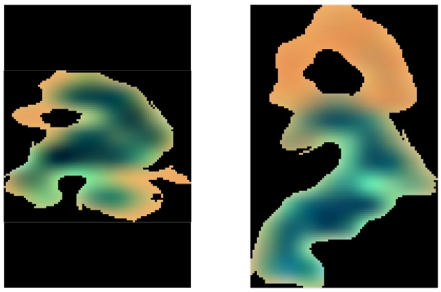

Fig. 3. X-ray images of a sample debris fragment from the "A" view (left) and "B" view (right) scans.

Subsequent extraction confirmed the debris as copper, underscoring the potential of color analysis in debris images as a valuable tool for material identification and to improve the accuracy of a 3D representation of the debris based on the two views.

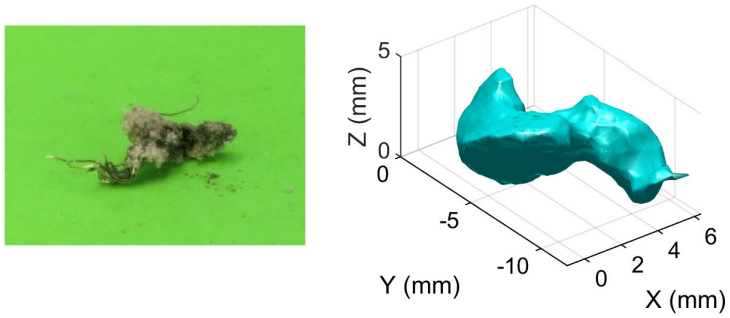

Fig. 4. Image of debris (left) and 3D model of debris (right) after extraction from foam panel.

Figure 4 is a projection of the real 3D scanned file. Rotating this image produces different projections. Such projections are denoted in polar co-ordinates as $I_{real}(\theta, \phi)$, where (θ, ϕ) are angles with respect to mutually orthogonal axes and are subject to change. The A view and B view images can be denoted as $X_{A_{view}}(\theta_{c1}, \phi_{c1}), X_{B\_view}(\theta_{c2}, \phi_{c2})$ where $\theta_{c1}, \ldots \phi_{c2}$ are constant angles since the views are of a stationary image. Mean squared error (MSE) between a cross-sectional view of real 3D scans of the debris and A view can be written as in Eq. 1, where (i, j) are pixel locations and (M, N) are dimensions of the photos. MSE is computed for each possible (θ, ϕ) value, then the angles with the least MSEs are stored.

$$\text{MSE}\left(I_{real}, X_{A_{view}}\right) \frac{1}{MN} \sum_{i=1}^{M} \sum_{j=1}^{N} \left(I_{real}(i,j) - X_{A_{view}}(i,j)\right)^2 \quad (1)$$

The image $I_{real}(\theta_{least\_MSE}, \phi_{least\_MSE})$ corresponds to the best possible projection of the 3D scan of the debris from the A view image of the debris. This process is repeated for B view as well. The x-ray images and their closest projections are shown in Fig. 5. The two projections of the 3D scan are approximately 55° apart, matching the angle between the views captured in the x-ray.

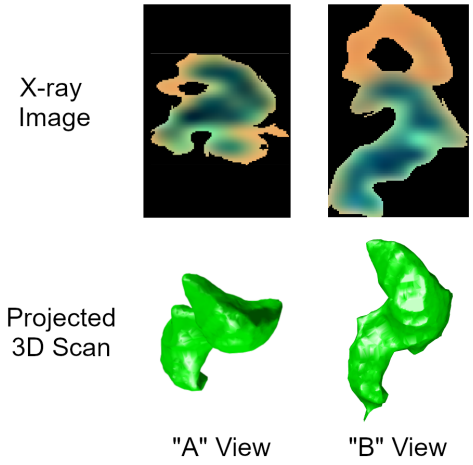

Fig. 5. Side-by-side comparison of x-ray debris images and their closest true projection.

From the comparison in Fig. 5, the x-ray views give a good representation of the shape and size of the imaged fragment. The color lightness values in the image also show a good correlation with the projected thickness of the real fragment.

3 Machine Learning – Predictive Model Development

3.1 Random Forest Classifier

The Random Forest Classifier was selected for modeling, due to a limitation in fully processed fragments with the x-ray image locations. Random Forest's ensemble nature, which combines multiple decision trees, captures complex non-linear relationships. Hyperparameter tuning was performed for performance optimization, focusing on parameters such as the number of trees, maximum depth, and minimum samples per leaf. The tuning aimed to balance model complexity and generalization, avoiding overfitting, while maintaining the ability to capture intricate patterns in the data.

3.2 Feature Selection

Since random forests have a set number of feature inputs, tailoring them is how to increase performance. In this case, the features are extracted from the x-ray debris images only, due to the unavailability of real dimensional and color data for debris under 10 mm.

3.2.1 Feature Selection - Colors

Each debris x-ray image has a unique color distribution. As seen in Table 1, the false-color representation used by the scanner software is a great predictor of material type as different densities tend to have distinct color profiles.

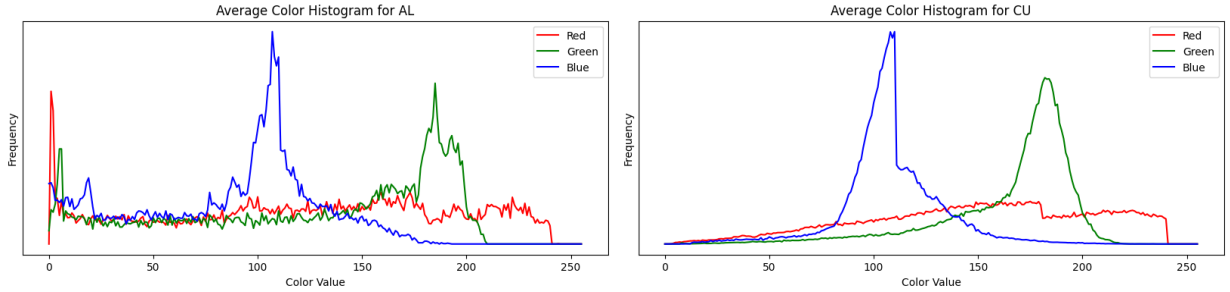

Fig. 6. Color histogram values for debris made of aluminum (left) and copper (right).

As seen in Fig. 6, blue and green color values throughout the debris image tend to concentrate on two specific values, while the red color for aluminum approaches zero. This occurs due to x-ray attenuation while imaging; therefore, 256 different values are divided into 32 bins with a range of 8 values each. The 32 bins include red, green, and blue values as a feature vector to the Random Forest Classifier.

3.2.2 Feature Selection - Shape

Shape is also an indicator of the debris type. From DebriSat related alone, it can be inferred that copper debris appears like wires since this was most of the mock satellite's copper. Table 2 lists the types of shape characteristics calculated and considered in the features vector.

Table 2. Description of Features of the X-ray Image Considered in the Classifier

Height and Width	**Dimensions of the fragment image in pixels**
Area	Area of the contour in pixels. Denoted by A.
Perimeter	Perimeter of the contour in pixels. Denoted by P.
Aspect Ratio $= \frac{W}{H}$	Measures the elongation of the debris and is defined as the ratio of the width to the height of the debris' bounding rectangle.
Extent $= \frac{A}{W \times H}$	Quantifies the compactness of the debris shape and is given by the ratio of the contour area to the area of the bounding rectangle.
Solidity $= \frac{A}{A_{\text{hull}}}$	Provides insight into the concavity of the debris shape. It is defined as the ratio of the debris contour area to the convex hull area.
Circularity $= \frac{4\pi A}{P^2}$	Quantifies how close the shape is to a circle, value 1 indicates perfect circle.
Eccentricity $= \sqrt{\frac{\lambda_1}{\lambda_2}}$	Quantifies deviation from being circular, computed from the eigenvalues (λ_1, λ_2) of the centralized second-moment matrix.

4 Material Classification - Results

The Random Forest Classifier is trained by dedicating 80% of the randomized debris data to model training with the remaining 20% for testing. Figure 7 represents the predictions for each material and represents counts of predicted and associated real material. The diagonals represent correct guesses.

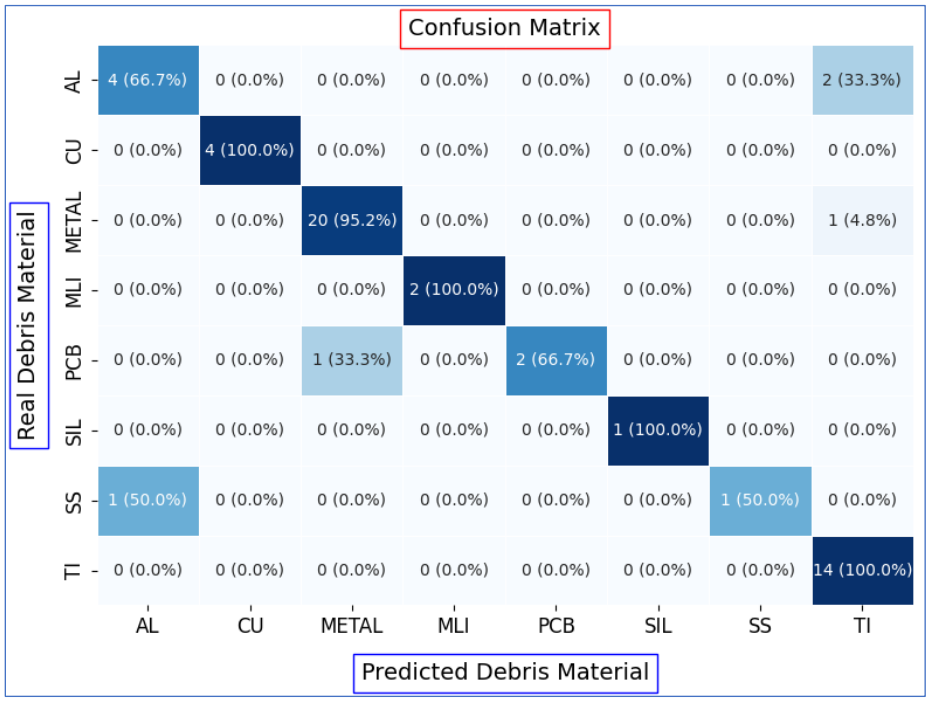

Fig. 7. Confusion matrix representing Random Forest Model predictions.

The confusion matrix shows model performance is best at identifying titanium with 100% accuracy for 14 instances. Reference [11] suggests all fragments labeled titanium in the database are actually stainless steel, and titanium was applied based on a biased calculation of fragment density. Given this, high accuracy of this algorithm in identifying titanium fragments is expected, since these fragments were previously mislabeled due to their irregular shape.

Table 3 shows overall accuracy of the algorithm. Precision here refers to the ratio of correct prediction to total prediction for each material, indicating model accuracy. Recall is the ability of the classifier to identify all instances of a material, defined as the ratio of true positives to the sum of true positives and false negatives. The F1-Score is the harmonic mean of precision and recall, providing a balanced single score taking both false positives and false negatives into account. Accuracy is a general overview of the model performance, representing the ratio of all correct predictions to the total number of instances.

It is evident that contour features play the most significant role when it comes to classifying the debris material type. Fig. 8 shows the relative importance of each feature in the classification. Additionally, some color ranges occurring in the images played a key role in determining material type and the perimeter as the highest contributing feature is of interest in patterns based on material.

Table 3. Model Accuracy Statistics

	Precision	**Recall**	**F1-Score**	**Support (test debris count)**
macro avg	0.95	0.85	0.88	53
weighted avg	0.91	0.91	0.90	53
Accuracy = 90.56 %				

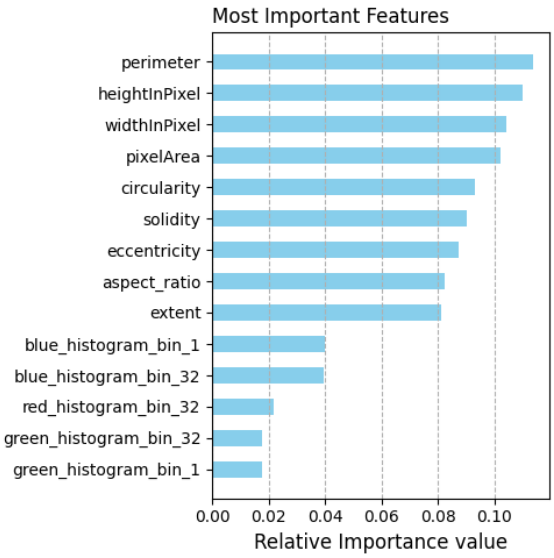

Fig. 8. The top features contributing towards the prediction algorithm.

5 Conclusions

In conclusion, this study demonstrates promising results in utilizing machine learning techniques to automate the characterization of small orbital debris fragments. The high accuracy achieved by the random forest model in categorizing material types from dual view x-ray images shows the feasibility of relying less on manual extraction and measurement. While challenges remain in reconstructing accurate 3D debris shapes due to imaging distortions, material predictions provide valuable data to supplement physical debris analysis. Applying these methods to infer material properties for the sub-10 mm DebriSat fragments will significantly augment the fundamental debris measurement dataset. Further work can build on this approach to optimize feature extraction and model performance. Overall, this represents an important step toward scalable integration of automated image analytics into orbital debris analysis pipelines.

6 Acknowledgements

The authors gratefully acknowledge the support and contributions of the Orbital Debris Program Office at NASA Johnson Space Center and University of Florida. Special thanks to James Murray for helping guide the theoretical framework and bestowing DebriSat specific knowledge. Special thanks to retired NASA DebriSat contributor Jack Bacon for his x-ray processing code, the backbone of this paper.

7 References

1. Rivero, M., *et al*. “Characterization of debris from the DebriSat hypervelocity test,” 66th International Astronautical Congress, Jerusalem, Israel, 2015.
2. Cowardin, H., *et al*. “Updates to the DebriSat Project in Support of Improving Breakup Models and Orbital Debris Risk Assessments,” Proceedings of the 2019 15th Hypervelocity Impact Symposium, 15th Hypervelocity Impact Symposium. Destin, FL, USA, April 14–19, 2019. V001T10A012. ASME.
3. Moraguez, M. “An Algorithm for Characteristic Length Measurement from Point Cloud Data,” AIAA Student Conference, Savannah, GA, 2015.

4. Scruggs, T. and Fitz-Coy, N. “Average Cross-Sectional Area of Idealized DebriSat Fragments Using Icosahedron Motivated Orientation Vectors,” Proc. 7th European Conference on Space Debris, Darmstadt, Germany, 18–21 April 2017.
5. Toledo, R., *et al*. “Imaging Systems Utilized in the DebriSat Fragment Size Characterization Process,” Proceedings of the First International Orbital Debris Conference, Sugar Land, TX, 2019.
6. Cowardin, H., *et al*. “Characterization of Orbital Debris via Hyper-Velocity Laboratory Based Tests,” 7th European Conference on Space Debris, Darmstadt, Germany, 2014.
7. Clark, S., *et al*. “Design of a representative LEO satellite and impact test for improved NASA satellite breakup modeling,” Proceedings of the 65th International Astronautical Congress, Toronto, Canada, 2014.
8. Bacon, J. B., *et al*. “X-Ray Imagery as the Record of All Data of Interest in Hypervelocity Impact Fragment Studies,” Proceedings of the 8th European Conference on Space Debris (virtual), 2021.
9. Kleespies, J. and Fitz-Coy, N. “DebriSat's DCS: A Database-Based Solution to the Big Data Challenges Impacting the Future Regulation of Orbital Debris,” 7th European Conference on Space Debris, Darmstadt, Germany, 18–21 April 2017.
10. Smiths detection HI-SCAN 5170-A User Manual (Page 72 of 222) | ManualsLib. https://www.manualslib.com/manual/1383291/Smiths-Detection-Hi-Scan-5170-A.html
11. Ondes, B., *et al.* “NASA DebriSat – Verification of Material Characterization Processes by utilization of Machine Learning Algorithms,” to be presented at the Second International Orbital Debris Conference, Sugar Land, TX, 2023.